CrossMark

ORIGINAL RESEARCH

New coordination modes of iminodiacetamide type ligands in palladium(II) complexes: crystallographic and DFT studies

Neven Smrečki[1] · Boris-Marko Kukovec[1] · Igor Rončević[1] · Zora Popović[1]

Abstract The reactions of N-alkyliminodiacetamide derivatives, namely N-ethyliminodiacetamide ($CH_3CH_2N(CH_2CONH_2)_2$; Etimda) and N-isopropyliminodiacetamide ($(CH_3)_2CHN(CH_2CONH_2)_2$; i-Primda), with sodium tetrachloropalladate(II) in aqueous solutions were investigated. Three new palladium(II) complexes, $[Pd(Etimda_{-H})_2]\cdot 2H_2O$ (**1**), $[Pd(i\text{-}Primda_{-H})_2]\cdot 2H_2O$ (**2**) and $[PdCl_2(i\text{-}Primda)]$ (**3**), were obtained and characterized by X-ray structural analysis, infrared spectroscopy and thermal analysis (TGA). The square planar coordination environments around the palladium(II) ions in complexes **1** and **2** consist of two N,N'-bidentate N-alkyliminodiacetamidato ligands, with imino N atoms in *trans*-position. The complex **3** also exhibits a square planar coordination environment around Pd(II), but with two chloride ions and one neutral N-isopropyliminodiacetamide ligand bound in an N,O'-bidentate coordination mode. The described coordination modes, as well as the presence of deprotonated amide groups in ligands in **1** and **2**, are found for the first time in palladium(II) complexes with iminodiacetamide type ligands. The molecular geometries and infrared spectra of these three complexes were also modelled using DFT calculations, at the BP86-D3/def2-TZVPP/PCM level of theory. The RMSD values suggest a good agreement of the calculated and experimental geometries. A QTAIM analysis suggests a qualitative correlation between bond lengths and energy densities, also supported by an NBO analysis. The dimer interaction energy between complex units was estimated at about −15 kcal/mol for all complexes.

Keywords Palladium(II) · N-alkyliminodiacetamide · Crystal structure · IR spectroscopy · DFT calculations
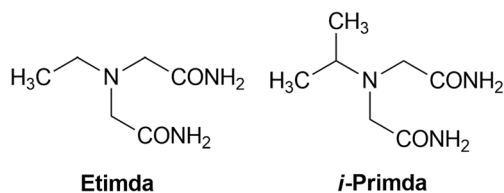
✉ Neven Smrečki
nsmrecki@chem.pmf.hr; neven.smrecki@gmail.com

✉ Boris-Marko Kukovec
bkukovec@chem.pmf.hr; borismarkokukovec@gmail.com

✉ Igor Rončević
ironcevic@chem.pmf.hr

[1] Department of Chemistry, Faculty of Science, University of Zagreb, Horvatovac 102a, 10000 Zagreb, Croatia

Introduction

An iminodiacetamide, $HN(CH_2CONH_2)_2$ (imda), is an amide derivative of the well-known complexone iminodiacetic acid, $HN(CH_2COOH)_2$ (idaH₂) [1]. Being a neutral ligand, iminodiacetamide forms cationic complexes with copper(II) and nickel(II), $[M(imda)_2]^{2+}$ (M = Cu(II) of Ni(II)) [2, 3], but neutral one with palladium(II), $[PdBr_2(imda)_2]$ [4]. The last one is, at the same time, the only example of a palladium(II) complex with iminodiacetamide type ligand that has been structurally described until now. This is surprising, since palladium(II) complexes are known to be highly efficient catalysts in modern synthetic organic chemistry [5, 6] and many of them also show remarkable antitumor potential [7]. Transition metal complexes with N-alkyliminodiacetamides and structurally related ligands [8–20] are generally scarce in the literature.

In order to get more insight into coordination chemistry of the palladium(II) complexes with iminodiacetamide type ligands, we have prepared three new palladium(II) complexes with N-ethyliminodiacetamide and N-isopropyliminodiacetamide (Scheme 1): $[Pd(Etimda_{-H})_2]\cdot 2H_2O$ (**1**), $[Pd(i\text{-}Primda_{-H})_2]\cdot 2H_2O$ (**2**) and $[PdCl_2(i\text{-}Primda)]$ (**3**). These complexes significantly differ

🌳 Springer

Scheme 1 Structural formulae of the ligands: *N*-ethyliminodiacetamide (Etimda) and *N*-isopropyliminodiacetamide (*i*-Primda)

from [PdBr$_2$(imda)$_2$], the only palladium(II) complex with iminodiacetamide type ligand reported by now [4], which contains a neutral ligand bound in an *N*-monodentate fashion via imino N atom of imda ligand. For the first time, the palladium(II) complexes with deprotonated amide groups of iminodiacetamide type ligands (Etimda in **1** and *i*-Primda in **2**) were reported, exhibiting an *N,N'*-bidentate coordination mode of iminodiacetamide type ligands. The complex **3** also differs from [PdBr$_2$(imda)$_2$] and both **1** and **2**, as it contains neutral *i*-Primda ligand bound in an *N,O'*-bidentate coordination mode. The studies based on comparison of experimental and calculated molecular structures and infrared spectra of the palladium(II) complexes with iminodiacetamide type ligands have not been reported in literature until now.

Experimental

Materials and physical measurements

All chemicals for the syntheses were purchased from commercial sources (Sigma-Aldrich, Acros Organics or Alfa Aesar) and used as received without further purification. The ligands were prepared as previously reported [11]. The CHN analyses were performed on a Perkin-Elmer 2400 Series II CHNS analyzer in the Analytical Services Laboratories of the Ruđer Bošković Institute, Zagreb, Croatia. The FTIR spectra were obtained in the range 4000–400 cm^{-1} on a Perkin-Elmer Spectrum Two™ FTIR-spectrometer in the ATR mode. The TGA measurements were performed at a heating rate of 10 °C min^{-1} in the temperature range of 25–600 °C, under oxygen flow of 150 mL min^{-1} on a Mettler-Toledo TG/SDTA 851^e instrument. Approximately 10 mg of sample was placed in a standard aluminium crucible (40 μL).

Synthesis of the complexes [Pd(Etimda$_{-H}$)$_2$]·2H$_2$O (1) and [Pd(*i*-Primda$_{-H}$)$_2$] · 2H$_2$O (2)

The ligand (1 mmol) was added to an aqueous solution of Na$_2$PdCl$_4$·xH$_2$O ($x ≈ 3$) (0.17 g; 0.5 mmol in 40 mL) and the mixture was heated to 80 °C, after which a clear red-orange solution was obtained. Sodium hydrogencarbonate (0.08 g; 1 mmol) was then added with stirring and the solution became yellow. Yellow crystals of **1** and **2**, suitable for X-ray structural analysis, were obtained by standing of the above-described reaction mixtures for 1 day at room temperature. The complexes were filtered off, washed with water (10 mL) and dried in air.

[Pd(Etimda$_{-H}$)$_2$]·2H$_2$O (**1**): From 0.16 g Etimda. Yield: 0.17 g (74%). *Anal.* Calc. for C$_{12}$H$_{28}$N$_6$O$_6$Pd (458.80): C 31.41, H 6.15, N 18.32%. Found: C 31.51, H 6.28, N 18.19%. IR data (cm^{-1}): 3381(s), 3326(s, br), 3274(s), 3077(w), 2985(w), 2952(w), 1688(s), 1634(m), 1589(vs), 1465(w), 1441(m), 1426(m), 1410(m), 1385(w), 1372(w), 1340(w), 1319(w), 1300(m), 1272(w), 1164(w), 1132(w), 1103(w), 1066(w), 1016(w), 976(w), 954(w), 920(w), 892(w), 848(w), 793(w), 750(w), 702(w), 677(w), 581(w), 519(w), 465(w).

[Pd(*i*-Primda$_{-H}$)$_2$]·2H$_2$O (**2**): From 0.17 g *i*-Primda. Yield: 0.19 g (77%). *Anal.* Calc. for C$_{14}$H$_{32}$N$_6$O$_6$Pd (486.85): C

Table 1 The crystallographic data for **1–3**

Compound	1	2	3
Formula	C$_{12}$H$_{28}$PdN$_6$O$_6$	C$_{14}$H$_{32}$PdN$_6$O$_6$	C$_7$H$_{15}$PdCl$_2$N$_3$O$_2$
M_r	458.80	486.85	350.52
Crystal system, space group	Monoclinic, $P2_1/n$ (No. 14)	Monoclinic, P2$_1$/n (No. 14)	Monoclinic, P2$_1$/c (No. 14)
a (Å)	7.9612(2)	8.2024(3)	12.1507(6)
b (Å)	9.0674(2)	8.9761(3)	7.0560(3)
c (Å)	12.8493(4)	13.2493(3)	15.1657(6)
β (°)	105.286(3)	98.678(3)	108.794(5)
V (Å^3)	894.74(4)	964.32(5)	1230.91(10)
Z	2	2	4
D_{calc} (g cm^{-3})	1.703	1.677	1.891
μ (mm^{-1})	1.079	1.007	1.927
R [$I \geq 2\sigma(I)$]	0.0189	0.0491	0.0252
wR [all data]	0.0470	0.2433	0.0649

Scheme 2 Preparation of palladium(II) complexes with *N*-alkyliminodiacetamide derivatives
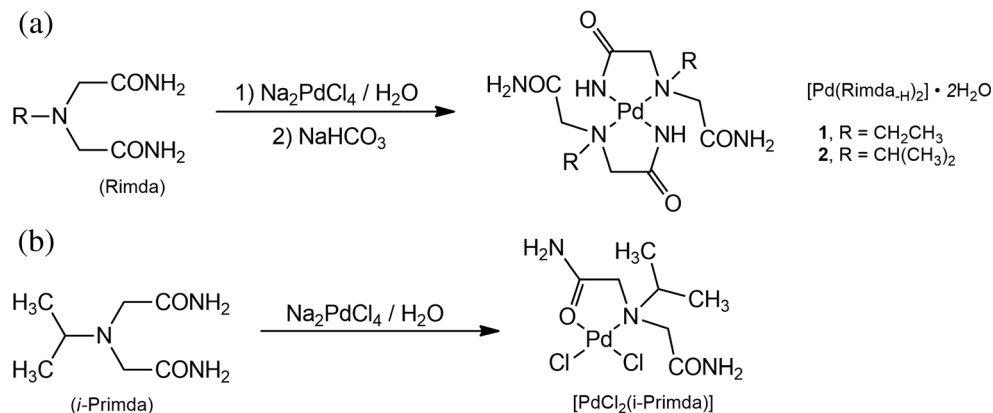
34.54, H 6.62, N 17.27%. Found: C 34.76, H 6.88, N 17.09%. IR data (cm^{-1}): 3422(m, br), 3334(s), 3217(s, br), 3094(s, br), 3005(w), 2988(m), 2954(w), 1686(vs), 1650(m), 1589(vs), 1463(w), 1439(m), 1427(m), 1409(m), 1395(m), 1372(w), 1340(w), 1315(m), 1276(m), 1265(m), 1177(w), 1152(m), 1133(m), 1072(w), 1030(w), 996(w), 949(w), 917(w), 902(w), 800(m), 749(w), 720(m), 688(w), 665(m), 597(m), 561(w), 529(w), 482(w).

Synthesis of the complex [PdCl₂(*i*-Primda)] (3)

The ligand (1 mmol; 0.17 g) was added to an aqueous solution of Na₂PdCl₄·*x*H₂O (*x* ≈ 3) (0.34 g; 1 mmol in 40 mL) and the mixture was heated for few minutes, until a clear

red-brown solution was obtained. Red-brown crystals of the product, suitable for X-ray structural analysis, were obtained by the slow evaporation of the reaction mixture for 1 week. The product was filtered off and washed with water (10 mL). Yield: 0.25 g (71%). *Anal.* Calc. for C₇H₁₅N₃O₂Cl₂Pd (350.52): C 23.98, H 4.31, N 11.99%. Found: C 24.16, H 4.40, N 12.11%. IR data (cm^{-1}): 3371(s, br), 3307(m), 3231(m), 3131(m), 2993(w), 2977(w), 2965(w), 1676(vs), 1652(vs), 1603(m), 1572(s), 1482(w), 1461(w), 1436(w), 1416(m), 1396(w), 1376(w), 1362(w), 1332(w), 1314(m), 1260(w), 1175(w), 1148(w), 1132(w), 1061(w), 1035(w), 983(w), 951(w), 935(w), 906(w), 895(w), 879(w), 807(w), 754(w), 704(w), 630(w), 608(w), 578(m), 508(w).

Fig. 1 ORTEP-style plots of [Pd(Etimda$_{-H}$)₂]·2H₂O (**1**) (**a**), [Pd(*i*-Primda$_{-H}$)₂]·2H₂O (**2**) (**b**) and [PdCl₂(*i*-Primda)] (**3**) (**c**) with a labelling scheme of the asymmetric unit. Thermal ellipsoids are drawn at 50% probability level at 296(2) K
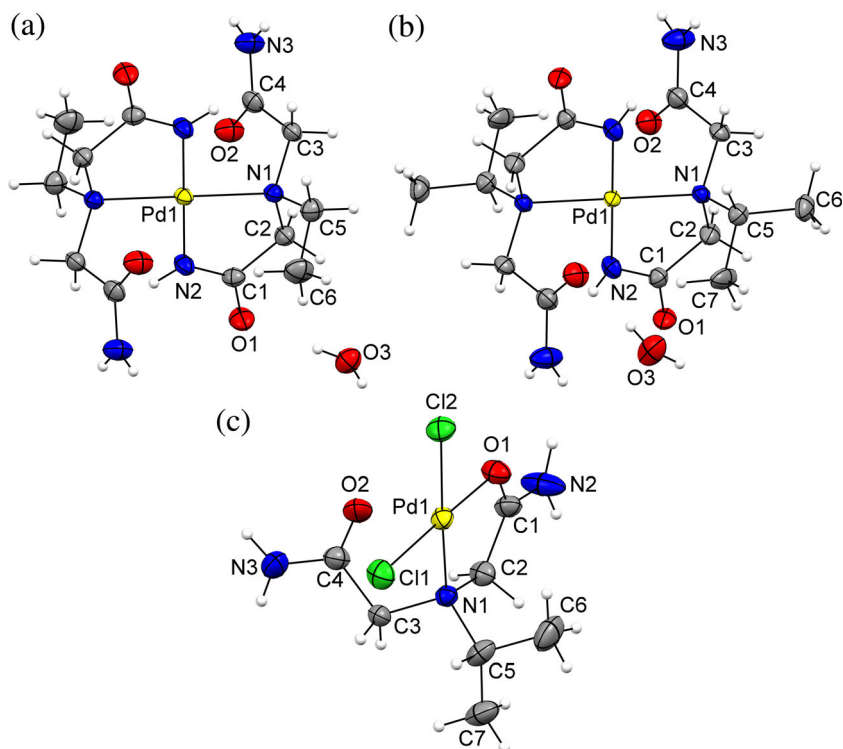
Table 2 The selected bond lengths (Å) and angles (°) for the experimental and calculated structures of **1–3**. The RMSD values are given for all bond lengths (including two hydrogen bonds for **1** and **2**) and all bond angles, with hydrogens excluded

	1		**2**			**3**	
Bond lengths	Exp	Calc	Exp	Calc	Bond lengths	Exp	Calc
Pd1–N1	2.079(2)	2.106	2.075(5)	2.114	Pd1–Cl1	2.2702(9)	2.301
Pd1–N2	1.995(2)	2.012	2.015(5)	2.009	Pd1–Cl2	2.2988(8)	2.312
Pd1–N1'	2.079(2)	2.106	2.075(5)	2.113	Pd1–N1	2.080(2)	2.121
Pd1–N2'	1.995(2)	2.012	2.015(5)	2.012	Pd1–O1	2.028(2)	2.053
C4–N3	1.323(3)	1.339	1.327(9)	1.345	C4–N3	1.327(5)	1.354
C4–O2	1.231(3)	1.250	1.239(8)	1.245	C4–O2	1.229(4)	1.238
RMSD (bond lengths)		0.0180		0.0246	RMSD (bond lengths)		0.0199
Bond angles					Bond angles		
N1–Pd1–N1'	180.00	178.59	180.0	179.48	Cl1–Pd1–Cl2	90.52(3)	92.25
N1–Pd1–N2'	97.77(7)	98.10	97.8(2)	98.28	O1–Pd1–Cl1	176.97(6)	174.20
N1–Pd1–N2	82.23(7)	81.79	82.2(2)	81.85	N1–Pd1–Cl2	176.76(7)	174.42
N2–Pd1–N2'	180.00	178.75	180.0	179.86	O1–Pd1–Cl2	92.46(6)	91.04
N3–C4–O2	123.5(2)	123.58	122.6(6)	123.06	O1–Pd1–N1	84.31(9)	83.51
					N1–Pd1–Cl1	92.72(7)	93.07
					N3–C4–O2	122.9(3)	123.95
RMSD (bond lengths)		1.05		1.49	RMSD (bond angles)		1.45

Symmetry code ('): −x + 1, −y + 1, −z + 1 (**1**) or −x + 1, −y + 1, −z (**2**)

X-ray crystallographic analysis

The suitable single crystal of **1–3** was selected and mounted in Paratone-N oil onto a thin glass fibre. The data collection was carried out on an Oxford Diffraction Xcalibur four-circle kappa geometry diffractometer with Xcalibur Sapphire 3 CCD detector, using a graphite monochromated MoKα (λ = 0.71073 Å) radiation at room temperature (296(2) K) and by applying the CrysAlisPro Software system, Version 1.171.37.35 [21]. The data reduction and cell refinement were performed by the same program. The structures were solved by SHELXS-2014 and refined by SHELXL-2014 [22]. The refinement procedure was done by full-matrix least-squares methods based on F^2 values against all reflections. The figures

were made with MERCURY (Version 3.5.1) [23]. The crystallographic data for **1–3** are summarized in Table 1.

Computational details

In our previous work, the BP86-D3/6-311 + G(d,p)/SDD level of theory was used to model IR spectra of similar compounds [24]. For complexes modelled in this work, the ECP basis set did not prove useful, as too much mixing between the ECP orbitals and valence orbitals was detected, which resulted in problems with SCF convergence. Instead, we used Alrichs' balanced def2 basis sets [25, 26]. First, a well-behaved wave function was constructed using a single-point BP86-D3/def2-TZVP calculation. This result was then used as a guess wave
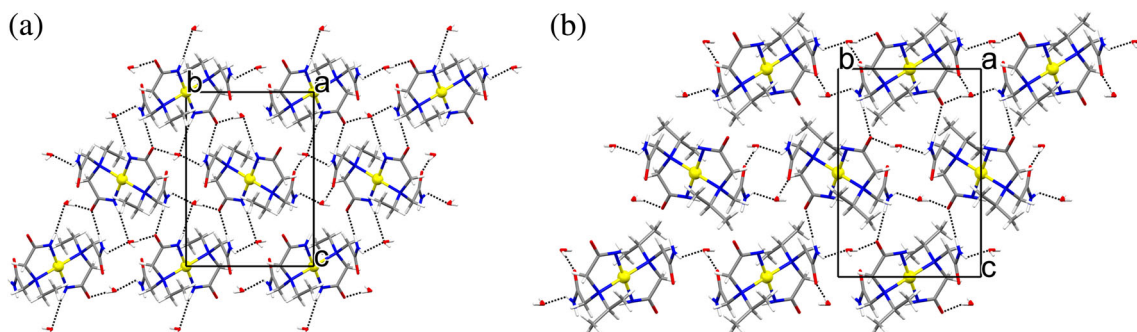

Fig. 2 The packing diagrams of [Pd(Etimda$_{-H}$)$_2$]·2H$_2$O (**1**) (**a**) and [Pd(*i*-Primda$_{-H}$)$_2$]·2H$_2$O (**2**) (**b**) (a view in the (1 0 0) plane). The molecules of [Pd(Etimda$_{-H}$)$_2$] (**a**) or [Pd(*i*-Primda$_{-H}$)$_2$] (**b**) and

water molecules of crystallization are assembled together into an infinite 3D framework by intermolecular N–H⋯O and O–H⋯O hydrogen bonds (shown by the *dotted lines*)

Table 3 Hydrogen bond geometry for **1**–**3**

D–H⋯A	d(D–H)/Å	d(H⋯A)/Å	d(D⋯A)/Å	∠(D–H⋯A)/°	Symmetry code on A
1					
N2–H21⋯O3	0.82(2)	2.33(2)	3.141(2)	172(2)	−x + 1/2, y − 1/2, −z + 3/2
N3–H31⋯O1	0.83(2)	2.02(2)	2.837(3)	169(3)	x + 1/2, −y + 3/2, z − 1/2
N3–H32⋯O3	0.83(2)	2.28(2)	2.906(3)	132(2)	−x + 1, −y + 2, −z + 1
O3–H31A⋯O1	0.82(2)	1.91(2)	2.723(2)	173(3)	x, y, z
O3–H32A⋯O2	0.81(2)	1.96(2)	2.767(2)	169(3)	x − 1, y, z
C2–H2A⋯O2	0.97	2.37	2.928(3)	116.1	x, y, z
2					
N3–H31⋯O1	0.86(1)	2.01(1)	2.864(7)	176(9)	x − 1/2, −y + 3/2, z + 1/2
N3–H32⋯O3	0.86(1)	2.30(5)	3.025(8)	142(8)	x − 1, y + 1, z
O3–H31A⋯O2	0.82(1)	2.07(2)	2.882(7)	173(8)	−x + 1, −y + 1, −z
O3–H32A⋯O1	0.82(1)	1.93(3)	2.723(7)	164(9)	−x + 2, −y + 1, −z
C2–H2B⋯O2	0.97	2.45	3.014(8)	116.9	x, y, z
C6–H6C⋯O3	0.96	2.60	3.514(9)	158.5	x, y + 1, z
3					
N2–H21⋯Cl1	0.86(2)	2.61(3)	3.343(4)	144(4)	x, −y + 1/2, z + 1/2
N2–H22⋯O2	0.86(2)	2.00(2)	2.841(4)	164(5)	−x + 1, −y + 1, −z + 1
N3–H31⋯Cl2	0.86(2)	2.52(2)	3.347(3)	161(4)	−x + 1, y − 1/2, −z + 1/2
N3–H32⋯Cl2	0.86(2)	2.48(2)	3.317(3)	166(4)	x, y − 1, z
C2–H2A⋯Cl1	0.97	2.73	3.551(3)	142.3	x, −y + 1/2, z + 1/2
C3–H3A⋯Cl1	0.97	2.81	3.282(3)	110.9	x, y, z
C5–H5⋯Cl1	0.98	2.77	3.395(4)	122.4	x, y, z

function for further calculations. The functionals BP86-D3, B3LYP-D3 and mPW1PW91 were tested, along with def2-TZVP and def2-TZVPP basis sets [27–31]. In cases where the conventional SCF procedure failed, the quadratically convergent SCF procedure was used [32].

The starting geometries for all modelled complexes were obtained from crystallographic data. As complexes **1** and **2** are hydrates, water molecules present in the crystal structure were
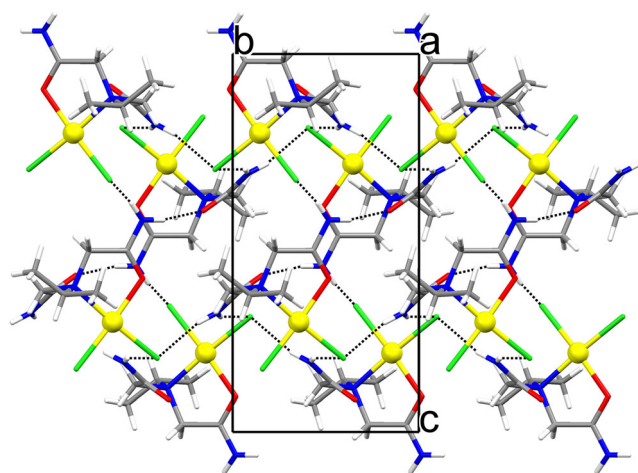

Fig. 3 The packing diagram of [PdCl₂(*i*-Primda)] (**3**). The [PdCl₂(*i*-Primda)] molecules are assembled into an infinite 2D network in the (1 0 0) plane by intermolecular N–H⋯O and N–H⋯Cl hydrogen bonds (shown by the *dotted lines*)

added to the geometries. In case of **3**, only a single monomer unit was considered. The optimizations were carried out both in vacuo and using the PCM model [33] and water as an implicit solvent, and were followed by frequency calculations carried out at the same level of theory. All calculations were performed using the Gaussian 09 program package [34].

QTAIM analysis was done on optimized geometries using AIMAll [35], while the single NBO calculations were performed with the NBO 6 program [36] at the BP86-D3/def2-TZVPP/PCM level of theory. Energies of interaction between two complex units were estimated at the same model chemistry by optimizing dimers of complexes, with the starting geometries taken from crystallographic data.

Results and discussion

Synthesis and general properties of the complexes

N-alkyliminodiacetamide derivatives contain three potential donor atoms, imino-nitrogen and two amide nitrogen or oxygen atoms. However, their reactions with sodium tetrachloropalladate(II) lead to the formation of complexes with different chemical composition and molecular geometry, depending on the reaction conditions. The reactions
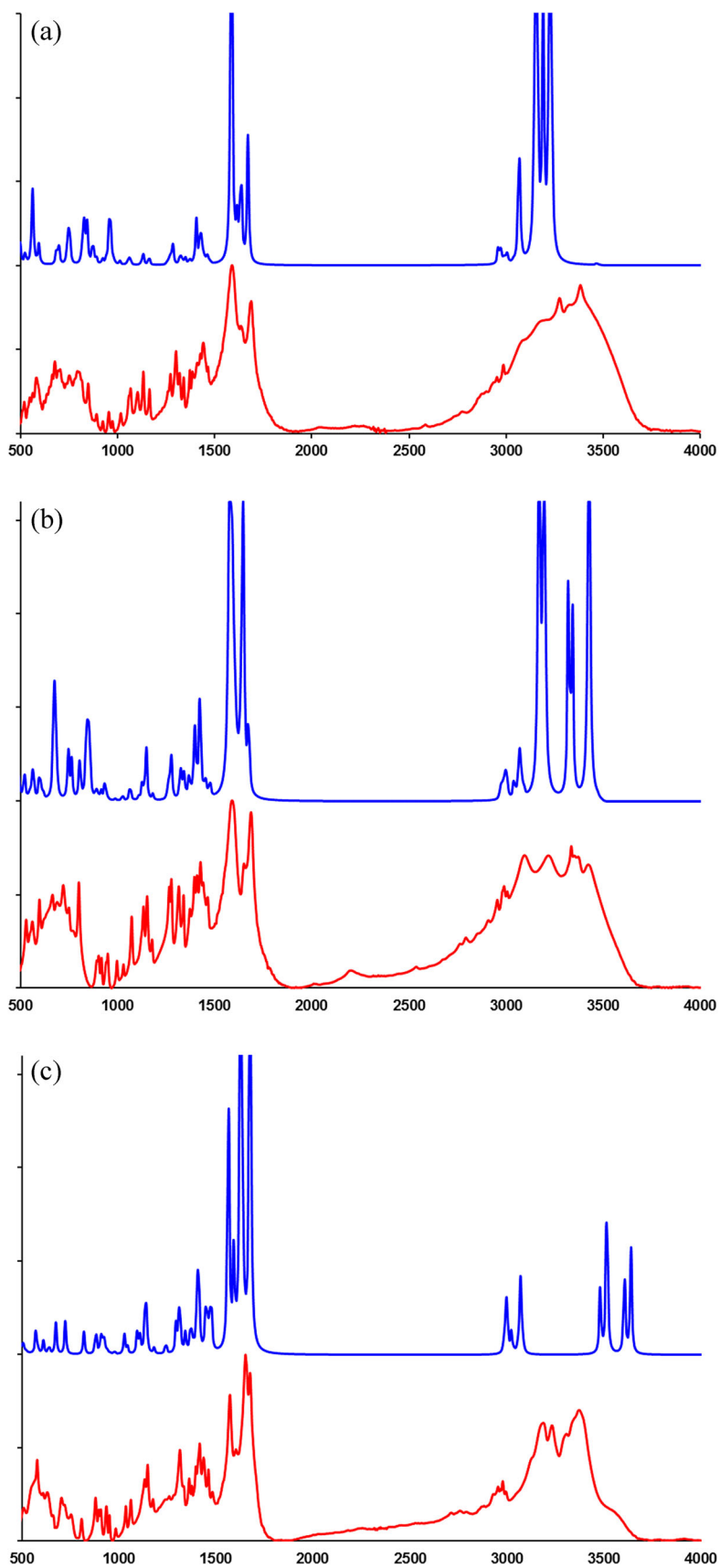
Fig. 4 The compared experimental IR spectra (cm^{-1}) of the complexes **1** (**a**), **2** (**b**) and **3** (**c**). Experimental spectra are shown in *red*, and predicted spectra in *blue*

of sodium(II) tetrachloropalladate(II) with these ligands and NaHCO$_3$ in molar ratio 1:2:2 (Scheme 2, a) resulted in formation of the complexes of the formula [Pd(Rimda$_{-H}$)$_2$]·2H$_2$O (R = Et or *i*-Pr). In the absence of any additional base, the reaction of Na$_2$PdCl$_4$ with *i*-Primda gave the complex [PdCl$_2$(*i*-Primda)] (Scheme 2, b), but no such complex could be isolated (possibly due to greater solubility) from the analogous reaction mixture containing Etimda instead of *i*-Primda.

All three complexes are stable substances which are practically insoluble in water. Thermal decomposition of **1** and **2** is characterized by dehydration above 100 °C and is finished around 150–170 °C. Complex **3**, as well as **1** and **2** after their dehydration, decompose in one step which corresponds to the loss of the coordinated ligands. The amount of undecomposed residue in oxygen atmosphere is in good accordance with the calculated amount of PdO. Full thermal analysis data for these complexes are given in Supplementary material.

Crystal structures

The palladium(II) ion is placed at the inversion centre and coordinated by two deprotonated *N,N′*-bidentate Etimda$_{-H}$ ligands in **1** or *i*-Primda$_{-H}$ ligands in **2**, resulting with the square planar coordination and the formation of *trans* isomers in both cases (∠(N1–Pd1–N1^i), 180° in **1** and **2**; symmetry code ('): −x + 1, −y + 1, −z + 1 (**1**) or −x + 1, −y + 1, −z (**2**)). The Etimda$_{-H}$ and *i*-Primda$_{-H}$ ligands are coordinated to palladium(II) ion via imino N1 and amide N2 atoms (Fig. 1a, b, Table 2). The τ$_4$ index [37] amounts 0 for both **1** and **2**. The palladium(II) ion in **3** is coordinated in a square planar fashion by a neutral *N,O′*-bidentate *i*-Primda ligand and two chloride atoms Cl1 and Cl2 in *cis* position (∠(Cl1–Pd1–Cl2), 90.52(3)°). The *i*-Primda ligand is coordinated via imino N1 and amide O1 atoms (Fig. 1c, Table 2). The τ$_4$ index for **3** amounts 0.04 indicating almost perfect square planar geometry.

The crystal packings of **1** and **2** are very similar. The molecules of [Pd(Etimda$_{-H}$)$_2$] (in **1**) or [Pd(*i*-Primda$_{-H}$)$_2$] (in **2**) and water molecules of crystallization in the respective crystal structures are assembled together into an infinite 3D framework by intermolecular N–H···O and O–H···O hydrogen bonds (Fig. 2a, b, Table 3). Each [Pd(Etimda$_{-H}$)$_2$] molecule is hydrogen-bonded to four neighbouring [Pd(Etimda$_{-H}$)$_2$] molecules and to eight neighbouring water molecules, while each water molecule is hydrogen-bonded to four neighbouring [Pd(Etimda$_{-H}$)$_2$] molecules in the crystal structure of **1**. In the crystal structure of **2**, each [Pd(*i*-Primda$_{-H}$)$_2$] molecule is hydrogen-bonded to four neighbouring [Pd(*i*-Primda$_{-H}$)$_2$] molecules and to six neighbouring water molecules, while each water molecule is hydrogen-bonded to three neighbouring

[Pd(*i*-Primda$_{-H}$)$_2$] molecules. The [PdCl$_2$(*i*-Primda)] molecules in the crystal structure of **3** are assembled into an infinite 2D network in the (1 0 0) plane by intermolecular N–H···O and N–H···Cl hydrogen bonds (Fig. 3, Table 3). Each [PdCl$_2$(*i*-Primda)] molecule is hydrogen-bonded to seven neighbouring molecules.

Analysis and comparison of the experimental and calculated infrared spectra and structures

Infrared spectra of all three complexes in the solid state (Fig. 4) are characterized by the presence of very strong and sharp bands of carbonyl group stretching, ν(C=O) [38, 39]. Two bands were found in similar spectral regions in the spectra of **1** (1688, 1634 cm^{-1}), **2** (1686, 1650 cm^{-1}) and **3** (1676, 1652 cm^{-1}), indicating the presence of two non-equivalent carbonyl groups (coordinated and non-coordinated) in the molecules of these complexes. Two pairs of characteristic bands of medium intensity, assigned as antisymmetric (ν_a) and symmetric stretching (ν_s) of the amide NH$_2$ groups, were observed in the range of 3100–3400 cm^{-1} for complex **3**. However, only three such bands appeared in the spectra of **1** and **2** since one of the four amide hydrogen atoms is replaced by palladium atom upon complexation. Clearly, two types of spectra, belonging to one of two kinds of the complexes, can be distinguished. The indication of the water molecules of crystallization in the hydrates **1** and **2** is due to the appearance of a broad band of medium intensity, observed at 3381 cm^{-1} (**1**) and 3422 cm^{-1} (**2**), which was assigned as O−H stretching, ν(OH, H$_2$O). The band is absent in the spectra of anhydrous complex **3**.

Of all tested methods, BP86-D3/def2-TZVPP in implicit solvent showed best correlation with experimental spectral data. This is not surprising, as the BP86 functional in combination with Alrichs' basis sets and empirical dispersion corrections has been often used in recent publications [29, 40, 41]. The comparison of experimental and calculated spectra was done by analysing the signals between 800 and 3100 cm^{-1} from experimental spectra. The calculated harmonic vibrational frequencies were matched with experimental values using linear regression. In this way, a relationship $\upsilon_{exp} = (1.004 \pm 0.002)\upsilon_{calc} + (9 \pm 3)$cm^{-1} between experimental and calculated frequencies was obtained. This method produced a mean unsigned error of 8.8 cm^{-1} between experimental and predicted frequencies below 3100 cm^{-1}, as shown in Table 4. For frequencies above 3100 cm^{-1}, describing the vibrations of H bonded groups, the discrepancies were larger since only a single molecule of the modelled complex was included in the calculation. In case of compound **1**, the frequencies of peaks at 3381 (ν(OH)) and 3274 cm^{-1} (ν_s(NH$_2$), ν(OH)) were underestimated in silico by about

Table 4 Experimental and predicted (BP86-D3/def2-TZVPP/PCM) harmonic frequencies (cm^{-1}) for selected vibration modes of **1–3**

1		2		3		
Experimental	Predicted	Experimental	Predicted	Experimental	Predicted	Mode
3200–3600	3100–3300	3200–3600	3100–3500	3200–3600	3450–3650	ν(OH, NH, NH$_2$ (H bonds))
3077	3069	3094	3089	3131	3069	ν_{as}(CH$_2$, CH$_3$)
2985	2974	3005	2996	2993	3019	ν_s(CH$_2$, CH$_3$)
2952	2958	2988	2990	2977	2997	ν_s(CH$_2$, CH$_3$)
		2954	2969	2965	2984	
1688	1667	1686	1674	1676	1672	ν(C=O), d_{sci}(H$_2$O, NH$_2$)
1634	1633	1650	1642	1652	1626	
				1603	1587	
1589	1581	1589	1575			ν_{as}(C=O)
				1572	1559	ν(C=O), d_{sci}(H$_2$O, NH$_2$)
1465	1469	1463	1472	1482	1471	d_{sci}(CH$_2$, CH$_3$), d_{oop}(CH$_2$, CH$_3$)
1441	1453			1461	1463	
1426	1431	1427	1424	1436	1440	
1410	1421	1409	1417	1416	1405	
1386	1401	1395	1395	1396	1393	
1372	1386	1372	1372	1376	1372	
1340	1343	1340	1339	1362	1363	d_{oop}(CH$_2$, CH$_3$)
1319	1327	1315	1317	1332	1337	d_{wag}(CH$_2$)
				1314	1308	d_{wag}(CH$_2$)
1300	1317					d_{wag}(CH$_2$), d_{twi}(CH$_2$, CH$_3$)
1272	1280	1276	1273	1175	1176	d_{twi}(CH$_2$,CH$_3$), ν(C-N), d(NH,NH$_2$)
		1265	1269			
1164	1157	1152	1143	1175	1176	ν(C–N), ν(C–C), d_{twi}(CH$_2$, CH$_3$)
1132	1127	1072	1059	1148	1138	
1103	1115			1132	1130	
1066	1058			1061	1080	
976	965	996	982	1035	1038	ν(C–N), ν(C–C), d(CH$_2$, CH$_3$)
954	957	949	944	935	930	ν(C–N), ν(C–C), d_{rock}(CH$_2$, CH$_3$)
920	917	917	926	879	876	
848	864	902	909			

100 cm^{-1}, corresponding to 3230 and 3188 cm^{-1}. On the other hand, good agreement was found in case of **2**, where the experimental peaks at 3422 (ν(OH)), 3334 (ν_s(NH$_2$)) and 3217 cm^{-1} (ν(OH)) corresponded to 3426, 3318 and 3195 cm^{-1}, respectively. In case of anhydrous **3**, the errors were largest—the ν(NH) and ν(NH$_2$) frequencies
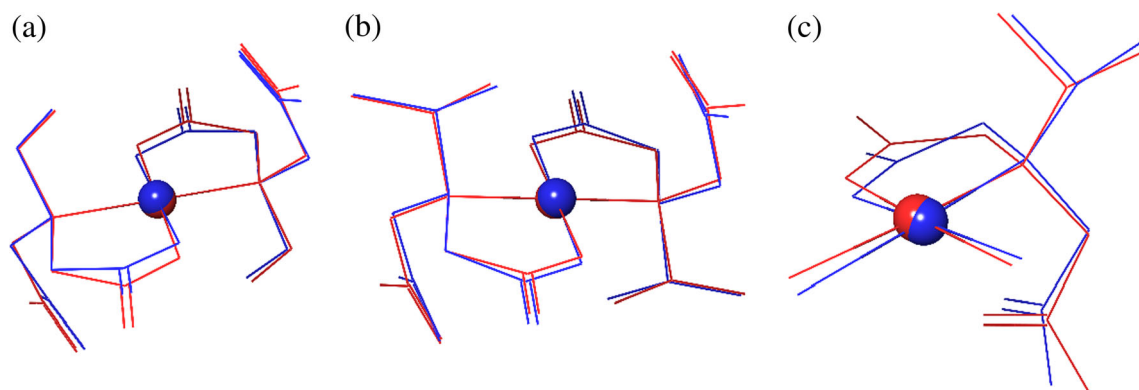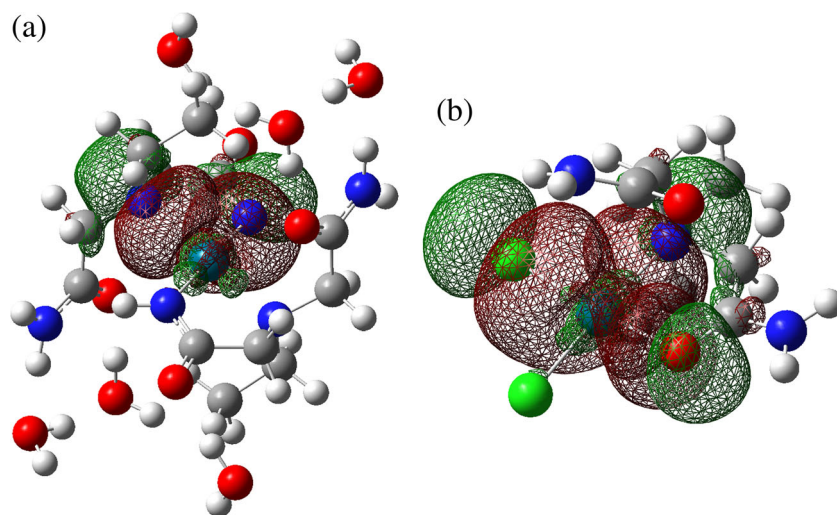

Fig. 5 An overlay between experimental (*red*) and calculated (*blue*) geometries of **1** (**a**), **2** (**b**) and **3** (**c**)

Fig. 6 Localized bonding Pd–N, Pd–Cl and Pd–O orbitals for **1** (**a**) and **3** (**b**). NBOs for **1** and **2** are very similar in shape, so only **1** is shown

were not dampened by any intramolecular interactions and thus were grossly overestimated.

Under 3100 cm^{-1}, the agreement was much better. All peaks corresponding to carbonyl stretching compounds were found in calculated spectra, with their intensities roughly corresponding to experimental ones (see Fig. 4). This trend remained in most of the other considered peaks describing the C–H, C–C and C–N

bends. The small errors there can be attributed to the lack of anharmonic corrections [42–44].

For further validation, structures obtained by optimization were compared to experimental ones. Their overlay is shown in Fig. 5, and the comparison between geometric parameters in Table 2. The obtained RMSD values show acceptable agreement, suggesting that a single molecule of the complex can be used in DFT calculations [45, 46].

Fig. 7 Results of QTAIM analysis for complexes **1** (**a**), **2** (**b**) and **3** (**c**). *Full lines* indicate stronger ($\rho_{BCP} > 0.025$) and *dashed lines* represent weaker $\rho_{BCP} < 0.025$ interactions. BCPs are shown in *green*

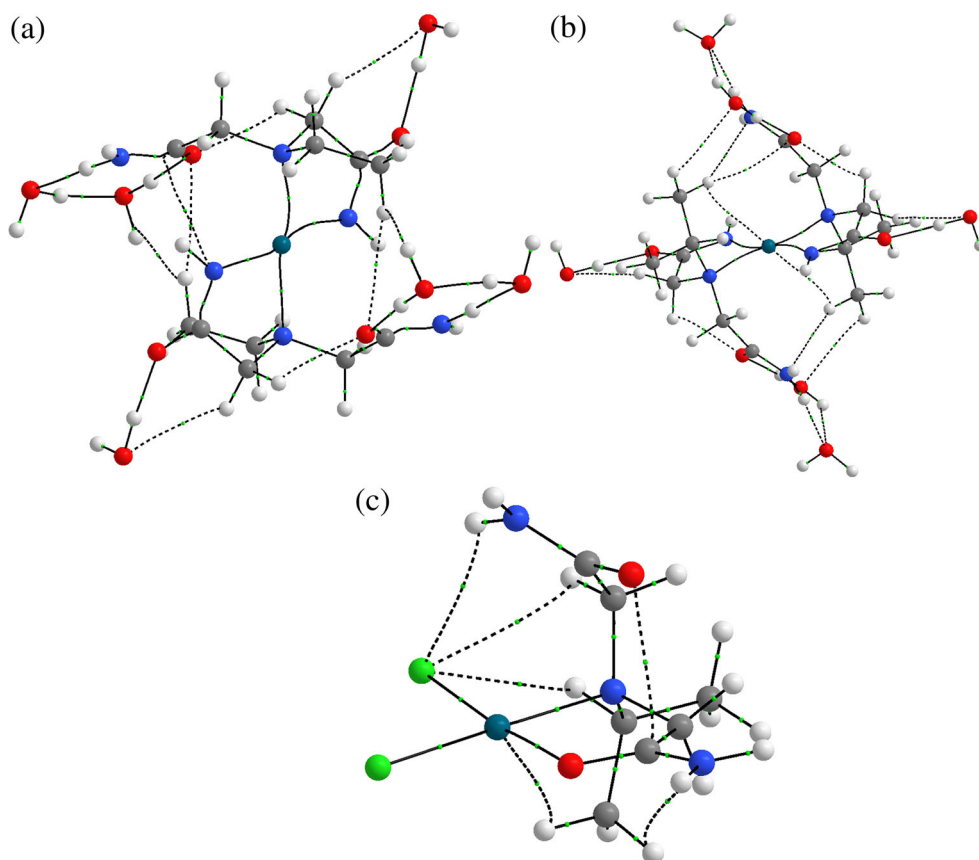**Table 5** Electron densities and Laplacian values in bond critical points for bonds between Pd and ligand donor atoms

Complex	Bond	ρ_{BCP}	$\nabla^2 \rho_{BCP}$
1	Pd1–N1	0.0942	0.337
	Pd1–N1'	0.0615	0.540
	Pd1–N2	0.1124	0.422
	Pd1–N2'	0.0759	0.710
2	Pd1–N1	0.0575	0.500
	Pd1–N1'	0.0575	0.505
	Pd1–N2	0.0712	0.660
	Pd1–N2'	0.0708	0.652
3	Pd1–N1	0.0946	0.315
	Pd1–O1	0.0940	0.429
	Pd1–Cl1	0.0893	0.226
	Pd1–Cl2	0.0870	0.221

Symmetry code ('): –x+1, –y+1, –z+1 (**1**) or –x+1, –y+1, –z (**2**)

QTAIM and NBO analysis

Using Natural Bond Orbital (NBO) analysis, the donor-acceptor relationship between the metal and the neighbouring ligands was further studied at the BP86-D3/def2-TZVPP/PCM level of theory. The relevant localized orbitals are shown in Fig. 6. Interaction energies between NBOs were calculated using second-order perturbative analysis of donor-acceptor interactions, E2PERT [47]. It suggests strong interactions between orbitals where N, O and Cl are the donors, while the acceptors are the vacant orbitals on Pd. For complexes **1** and **2**, the best donors are the nitrogen lone pair orbitals (150–100 kcal/mol for **1** and 50–100 kcal/mol for **2**), followed by

Pd–N bonding orbitals (25–40 kcal/mol). In case of complex **3**, nitrogen and oxygen are much better donors (55–60 kcal/mol) than chlorine (10–15 kcal/mol).

Bader's quantum theory of atoms-in-molecules (QTAIM) was used for a topological analysis of electronic density. In QTAIM, the electron density ρ values in bond critical points (BCPs) can be used to estimate the strength of the bond—ρ_{BCP} values on the order of 0.1 indicate a covalent (or similar strong) interaction, while weaker interactions (such as hydrogen bonds) typically have ρ_{BCP} values above 0.001 [48, 49].

Figure 7 and Table 5 show the results of the QTAIM analysis, done at the BP86-D3/TZVPP/PCM level of theory. Generally, all of the ρ_{BCP} values shown in Table 5 are consistent with strong coordinative bonds. Both in complexes **1** and **2**, the N2 and N2' atoms are more strongly bound to Pd than N1 and N1'. In complex **2**, the ρ_{BCP} values are larger than the corresponding ones in complex **1**, which is in agreement with the donor-acceptor stabilization energy trends obtained with E2PERT analysis. This is also observed in complex **3**, where the ρ_{BCP} values for N and O bonds are larger than for Cl1 and Cl2. Also, the ρ_{BCP} values are qualitatively correlated to bond lengths (shorter bonds correspond to larger ρ_{BCP} values), which was reported previously [50]. When considering hydrogen bonds between complexes and water molecules (present in **1** and **2**), all of the ρ_{BCP} values are between 0.0200 and 0.0300 and all the $\nabla^2 \rho_{BCP}$ values are positive, suggesting typical closed-shell interactions.

Complex dimerization energy estimation

As it can be seen from the above discussion, the modelling of a single unit of the complex can provide a lot of insight into its vibrational and electronic structure. However, the crystal

Fig. 8 Obtained structures for the dimers of **1** (**a**), **2** (**b**) and **3** (**c**). In **1** and **2**, the water molecules not important for dimer interactions are omitted for clarity
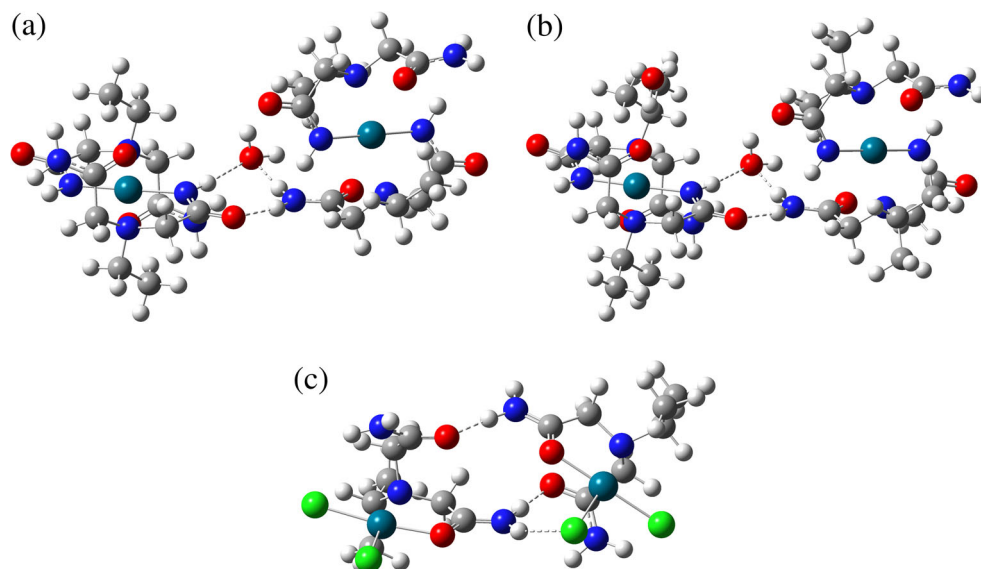
structure is largely influenced by the interactions between neighbouring complex units of the investigated molecule. In order to estimate the energy of interaction between two units of the complex, the energy of the reaction 2 **Complex** → (**Complex**)$_2$ was calculated using the energies obtained by optimization at the BP86-D3/def2-TZVPP level of theory with water as the implicit (PCM) solvent. In case of **1** and **2**, monomeric units with 6 water molecules (previously used for vibrational analysis) were fused, resulting in products with 12 water molecules, one of which bridges the two molecules of the complex. The dimer products are shown in Fig. 8. Obtained dimerization energies are similar: −17.26, −14.63 and −16.93 kcal/mol for compounds **1**, **2** and **3**, respectively. This is consistent with the formation of three new hydrogen bonds, as indicated in Fig. 8.

Conclusions

In the presence of a mild base, complexes [Pd(Etimda$_{-H}$)$_2$]·2H$_2$O (**1**) and [Pd(i-Primda$_{-H}$)$_2$]·2H$_2$O (**2**) were obtained, containing two deprotonated amide ligands bound in an N,N′-bidentate coordination mode. In the absence of a mild base, complex [PdCl$_2$(i-Primda)] (**3**) was produced, containing a neutral amide ligand bound in an N,O′-bidentate coordination mode. These coordination modes were found for the first time in palladium(II) complexes with iminodiacetamide type ligands, as the only known coordination mode in such type of complexes was N-monodentate via imino N atom [4]. Also, complexes **1** and **2** are the first palladium(II) complexes containing deprotonated amide groups of iminodiacetamide type ligands.

The substituents at imino N atom in the ligands (ethyl vs. i-propyl) do not have any influence on the kind of complexes prepared, as the type of complexes depends on the basicity of the reaction solution. Moreover, the substituents at imino N atom in the ligands do not have a significant influence on the crystal packings, apparent from very similar crystal structures of **1** and **2**. This is not very surprising, as ethyl and i-propyl groups are weak proton donors and participate only in weak hydrogen bonding, thus not affecting significantly the respective crystal packings of **1** and **2**. The complex molecules and water molecules of crystallization of **1** and **2** are assembled into 3D framework by a complex network of N–H···O and O–H···O hydrogen bonds, very similar to the crystal structures of [Pd(HBnida)$_2$]·2H$_2$O [51] and [Pd(i-PridaH)$_2$]·2H$_2$O [52]. However, in the case of **3**, molecules are connected into 2D network. This difference can be hardly attributed to the presence of weaker N–H···Cl hydrogen bonds in the crystal structure of **3**, but rather to the absence of water molecules of crystallization, leading to a less complicated structure due to the decrease of potential proton donors and acceptors.

The structure and spectra of the complexes were additionally validated using BP86-D3/def2-TZVPP/PCM level of theory. A very good agreement between experimental and DFT calculated results for both geometries and harmonic frequencies was achieved in the case of all three complexes.

References

1. Bell CF (1977) Principles and applications of metal chelation. Oxford Chemistry Series, Clarendon Press, Oxford University Press, Oxford
2. Sekizaki M (1974). Bull Chem Soc Jpn 47:1447–1450
3. Sekizaki M (1976). Acta Crystallogr B 32:1568–1570
4. Sekizaki M (1981). Bull Chem Soc Jpn 54:3861–3862
5. Clayden J, Greeves N, Warren S, Wothers P (2001) Organic chemistry. Oxford University Press, Oxford,
6. Tsuji J (2004) Palladium reagents and catalysts. Wiley, Chichester,
7. Abu-Surrah AS, Al-Sa'doni HH, Abdalla MY (2008). Cancer Therapy 6:1–10
8. Smrečki N, Kukovec B-M, Đaković M, Popović Z (2015). Polyhedron 93:106–117
9. Smrečki N, Stilinović V, Merkaš M, Lučić A, Kukovec B-M, Popović Z (2016). Aust J Chem 69:896–904
10. Smrečki N, Stilinović V, Jović O, Kukovec B-M, Popović Z (2017). Inorg Chim Acta 462:57–63
11. Smrečki N, Jović O, Molčanov K, Kukovec B-M, Kekez I, Matković-Čalogović D, Popović Z (2017). Polyhedron 130:115–126
12. Ran J-W, Pei J (2013). Acta Crystallogr E69:m325–m325
13. Deng X-H, Nie Q-J, Zhu F-J (2013). Acta Crystallogr E69:m89–m89
14. Clapp LA, Siddons CJ, Van Deerver DG, Reibenspies JH, Jones SB, Hancock RD (2006) Dalton Trans 2001–2007
15. Smith DA, Sucheck S, Pinkerton A (1992) J Chem Soc Chem Commun 367–368
16. Claudio ES, Horst MA, Forde CE, Stern CL, Zart MK, Godwin HA (2000). Inorg Chem 39:1391–1397
17. Clapp LA, Siddons CJ, Whitehead JR, Van Derveer DG, Rogers RD, Griffin ST, Jones SB, Hancock RD (2005). Inorg Chem 44:8495–8502
18. Burdinski D, Pikkemaat JA, Lub J, de Peinder P, Garrido LN, Weyhemuller T (2009). Inorg Chem 48:6692–6712
19. Krot K, Liamas-Saiz AL, Vembu N, Nollan KB (2007). Z Anorg Allg Chem 633:1900–1910
20. Skrzypczak-Jankun E, Smith DA (1994). Acta Crystallogr C50:1585–1588
21. CrysAlisPro (2014) Agilent Technologies, Yarnton, Oxfordshire, England. Version 1.171.37.35
22. Sheldrick GM (2008). Acta Crystallogr A64:112–122
23. Macrae CF, Bruno IJ, Chisholm JA, Edgington PR, McCabe P, Pidcock E, Rodriguez-Monge L, Taylor R, van de Streek J, Wood PA (2008). J Appl Crystallogr 41:466–470
24. Smrečki N, Rončević I, Popović Z (2016). Aust J Chem 69:1285–1291
25. Weigend F, Ahlrichs R (2005). Phys Chem Chem Phys 7:3297–2305
26. Weigend F (2006). Phys Chem Chem Phys 8:1057–1065
27. Cramer CJ, Truhlar DG (2009). Phys Chem Chem Phys 11:10757–10816
28. Steinmetz M, Grimme S (2013). ChemistryOpen 2:115–124

29. Raoufmoghaddam S, Mannathan S, Minnaard AJ, de Vries JG, Reek JN (2015). Chemistry 21:18811–18820

30. Goerigk L, Grimme S (2011). Phys Chem Chem Phys 13:6670–6688

31. Tsipis AC (2014). Coord Chem Rev 272:1–29

32. Schlegel HB, McDouall JJ (1991) In: Ögretir C, Csizmadia IG (eds) Computational advances in organic chemistry. Kluwer Academic, The Netherlands, pp. 167–185

33. Tomasi J, Mennucci B, Cammi R (2005). Chem Rev 105:2999–3093

34. Gaussian 09, Revision A.02, Frisch MJ, Trucks GW, Schlegel HB, Scuseria GE, Robb MA, Cheeseman JR, Scalmani G, Barone V, Petersson GA, Nakatsuji H, Li X, Caricato M, Marenich A, Bloino J, Janesko BG, Gomperts R, Mennucci B, Hratchian HP, Ortiz JV, Izmaylov AF, Sonnenberg JL, Williams-Young D, Ding F, Lipparini F, Egidi F, Goings J, Peng B, Petrone A, Henderson T, Ranasinghe D, Zakrzewski VG, Gao J, Rega N, Zheng G, Liang W, Hada M, Ehara M, Toyota K, Fukuda R, Hasegawa J, Ishida M, Nakajima T, Honda Y, Kitao O, Nakai H, Vreven T, Throssell K, Montgomery JA Jr, Peralta JE, Ogliaro F, Bearpark M, Heyd JJ, Brothers E, Kudin KN, Staroverov VN, Keith T, Kobayashi R, Normand J, Raghavachari K, Rendell A, Burant JC, Iyengar SS, Tomasi J, Cossi M, Millam JM, Klene M, Adamo C, Cammi R, Ochterski JW, Martin RL, Morokuma K, Farkas O, Foresman JB, Fox DJ (2016) Gaussian, Inc., Wallingford

35. AIMAll (Version 17.01.25), Todd A. Keith (2017) TK Gristmill Software, Overland Park KS, USA, (aim.tkgristmill.com)

36. NBO 6.0., Glendening ED, Badenhoop JK, Reed AE, Carpenter JE, Bohmann JA, Morales CM, Landis CR, Weinhold F (2013) Theoretical Chemistry Institute, University of Wisconsin, Madison

37. Yang L, Powell DR, Houser RH (2007) Dalton Trans 955–964

38. Silverstein RM, Webster FX, Kiemle D (2005) Spectrometric identification of organic compounds, 7th edn. Wiley, New York,

39. Nakamoto K (2009) Infrared and Raman spectra of inorganic and coordination compounds, part B, 6th edn. Wiley, Hoboken,

40. Pandey KK, Patidar P, Vishwakarma R (2014). Eur J Inorg Chem 18:2916–2923

41. Weymuth T, Couzijn EPA, Chen P, Reiher M (2014). J Chem Theory Comput 10:3092–3103

42. Pirc G, Stare J, Mavri J (2010). J Chem Phys 132:224506–224513

43. Stare J, Mavri J, Grdadolnik J, Zidar J, Maksić ZB, Vianello R (2011). J Phys Chem B 115:5999–6010

44. Brela M, Stare J, Pirc G, Sollner-Dolenc M, Wojcik MJ, Mavri J (2012). J Phys Chem B 116:4510–4518

45. Smrečki N, Jović O, Stilinović V, Kukovec B-M, Đaković M, Popović Z (2016). Inorg Chim Acta 453:95–103

46. Kukovec B-M, Kodrin I, Mihalić Z, Popović Z (2011). Inorg Chim Acta 378:154–162

47. Weinhold F (1998) Natural Bond Orbital Methods. In: Schleyer P v R (ed) Encyclopedia of Computational Chemistry, vol 3, pp. 1792–1811

48. Bader RFW (1990) Atoms in molecules: a quantum theory. Oxford University Press, Oxford,

49. Koch U, Popelier PLA (1995). J Phys Chem 99:9747–9754

50. Dimić D, Petković M (2015). Int J Quantum Chem 116:27–34

51. Smrečki N, Kukovec B-M, Jazwinski J, Liu Y, Zhang J, Mikecin A-M, Popović Z (2014). J Organomet Chem 760:224–230

52. Smrečki N, Kukovec B-M, Rotim K, Oršolić D, Jović O, Rončević T, Režić Mužinić N, Vinković M, Popović Z (2017). Inorg Chim Acta 462:64–74